PHOTONICS Research

Bismuth nanosheets as a Q-switcher for a mid-infrared erbium-doped SrF_2 laser

JINGJING LIU,[1] HAO HUANG,[2] FENG ZHANG,[2] ZHEN ZHANG,[3] JIE LIU,[1,4,*] HAN ZHANG,[2,6] AND LIANGBI SU[3,5,7]

[1]Shandong Provincial Key Laboratory of Optics and Photonic Devices, School of Physics and Electronics, Shandong Normal University, Jinan 250014, China
[2]SZU-NUS Collaborative Innovation Centre for Optoelectronic Science & Technology, and Key Laboratory of Optoelectronic Devices and Systems of the Ministry of Education and Guangdong Province, College of Optoelectronic Engineering, Shenzhen University, Shenzhen 518060, China
[3]CAS Key Laboratory of Transparent and Opto-Functional Inorganic Materials, Synthetic Single Crystal Research Center, Shanghai Institute of Ceramics, Chinese Academy of Sciences, Shanghai 201899, China
[4]Institute of Data Science and Technology, Shandong Normal University, Jinan 250014, China
[5]State Key Laboratory of High Performance Ceramics and Superfine Microstructure, Chinese Academy of Sciences, Shanghai Institute of Ceramics, Shanghai 201899, China
[6]e-mail: hzhang@szu.edu.cn
[7]e-mail: suliangbi@mail.sic.ac.cn
*Corresponding author: jieliu@sdnu.edu.cn

Received 6 April 2018; revised 3 May 2018; accepted 26 May 2018; posted 30 May 2018 (Doc. ID 327857); published 5 July 2018

Bismuth nanosheets (Bi-NSs) were successfully prepared and employed as saturable absorbers to generate a diode-pumped dual-wavelength Er^{3+}:SrF_2 laser in the mid-infrared region. *Q*-switched pulses with a maximum output power of 0.226 W were obtained at an absorbed pump power of 1.97 W. A repetition rate of 56.20 kHz and a minimum pulse duration of 980 ns were achieved. To the best of our knowledge, we present the first application of Bi-NSs in a mid-infrared all-solid-state laser. The results prove that Bi-NSs may be applied as an optical modulator in mid-infrared photonic devices or as a mode-locker and *Q*-switcher.

OCIS codes: (140.3380) Laser materials; (140.3500) Lasers, erbium; (140.3540) Lasers, Q-switched; (140.3580) Lasers, solid-state.

https://doi.org/10.1364/PRJ.6.000762

1. INTRODUCTION

Mid-infrared solid-state lasers have attracted increasing attention owing to their broad applications in the military, medical treatments, and air pollution monitoring [1,2]. Mid-infrared solid-state lasers have a low cost, simple structure, and rare-earth ions doped crystals as the gain medium. They are directly pumped by the laser diode (LD) and can thus effectively achieve miniaturization and high efficiency. Tm^{3+}, Er^{3+}, and Ho^{3+} are the main rare-earth ions emitting at 2–5 μm in the mid-infrared region [3–7]. Indeed, Er^{3+}-doped lasers have efficient emissions involving a transition from the $^4I_{11/2}$ to the $^4I_{13/2}$ state around 2.8 μm, which is in the strong absorption region of water. They are thus an ideal pumping source for mid-infrared and far-infrared optical parametric oscillations (OPOs) [8].

However, the lifetime of the upper laser energy level (Er^{3+}:$^4I_{11/2}$) is always shorter than that of the lower laser energy level (Er^{3+}:$^4I_{13/2}$) in 2.8 μm Er^{3+}-doped laser materials. This phenomenon is known as the self-terminating process. Generally, this problem can be easily solved. Improving the doping concentration of Er^{3+} is one effective way to achieve the desired laser output: with the increase in Er^{3+} doping concentrations, the lifetime of Er^{3+}:$^4I_{13/2}$ decreases faster than that of Er^{3+}:$^4I_{11/2}$ owing to the cross relaxation between the two levels. Furthermore, codoping with deactivating ions such as Pr^{3+} and Nd^{3+} is another effective way to depopulate the Er^{3+}:$^4I_{13/2}$ level [9–11]. However, only few studies have reported successful laser outputs. In SrF_2 and CaF_2 crystals, the trivalent rare-earth ions tend to form clusters even at low doping concentrations [12]. Furthermore, the phonon energy is lower in fluoride materials than in oxide materials, which can greatly reduce the probability of nonradiative transitions [13].

In recent years, two-dimensional (2D) materials have attracted much attention owing to their outstanding properties and widespread applications, particularly as optical modulators in pulse lasers. Owing to the large operating bandwidth, controllable bandgap, and easy fabrication method, 2D materials, including the graphene family [14–19], transition metal dichalcogenides [20–23], topological insulators [24–28], phosphorus [29–34], and the recently discovered MXene [35] and antimonene [36,37], have been considered as low-cost substitutes for saturable absorbers (SAs) in semiconductor saturable absorber mirror (SESAM) devices. Bismuth nanostructures, a novel 2D

material, show unique electronic and optical properties. With their moderate bandgap, high carrier mobility, and high stability at room temperature, bismuth nanostructures have become an increasingly interesting topic of discussion for researchers [38]. The saturable absorption property of bismuthene was first demonstrated in a 1559 nm fiber laser by Lu *et al.* [39]. However, to the best of our knowledge, the application of bismuth nanosheets (Bi-NSs) as an SA in the mid-infrared spectral region has not been reported.

In this work, by using Bi-NSs as an SA, a stable passively Q-switched Er^{3+}:SrF_2 laser was obtained. The saturable absorption behavior of Bi-NSs is demonstrated at 2.8 μm. In addition, this study provides a detailed analysis of the passively Q-switched laser, including the variation of output power, pulse width, and repetition rate under different transmissions of output mirrors.

2. CHARACTERIZATIONS OF THE BI-NSs SA AND EXPERIMENTAL SETUP

The Bi-NSs were synthesized from bismuth powder using a sonication method. In a typical procedure, 200 mg of bismuth powder was added into a glass bottle with 100 mL of pure N-methylpyrrolidone (NMP), followed by 6 h in an ice bath (SBL-22DT, with a power of 70% of 600 W). Then, the solution was probe sonicated for 24 h (BILON-1800Y, with a power of 60% of 1800 W) and kept in an ice bath for another 6 h. After that, the solution was centrifuged for 20 min at a speed of 3000 r/min. The supernatant was collected and centrifuged for another 20 min at a speed of 7000 r/min, and the Bi-NSs were finally obtained as the precipitate. The precipitate was washed twice with deionized water. Then, trichloromethane was added, and the solution was obtained after ultrasonication for 2 h. Finally, 100 μL of solution was spin coated at a speed of 1000 r/min for 15 s for the uniform adhesion of the Bi-NSs on fused quartz plates (JGS3 with 1 mm thickness). The structure of the Bi-NSs was confirmed by high-resolution transmission electron microscopy (HRTEM), as shown in Fig. 1(a). The Raman spectrum of Bi-NSs is shown in Fig. 1(b). Two peaks near 69 and 95 cm^{-1} are indicative of the bismuth structure, which correspond to an earlier report [40]. To identify the thickness of the Bi-NSs, the atomic force microscopy (AFM) was taken. As shown in Figs. 1(c) and 1(d), the AFM image shows that the thickness of the Bi-NSs was no more than 2.5 nm.

The nonlinear absorption mechanism of the Bi-NSs has been described in detail in Ref. [38]. The nonlinear optical properties of Bi-NSs SA were characterized by Z-scan method with a nanosecond pulsed laser at 2.8 μm. The repetition rate is 50 kHz, and the pulse duration is 50 ns. The beam waist was about 60 μm, and the Rayleigh length was about 0.2 mm. The transmittance has a relation with the input optical intensity by the formula [41]

$$T = 1 - \frac{\alpha_s}{1 + I/I_s} - \alpha_{\mathrm{ns}}, \tag{1}$$

where α_s is the saturable absorption, also defined as the modulation depth, α_{ns} is the nonsaturable loss, and I_s is the saturable intensity. By fitting the experimental data, the nonlinear transmittance curve is shown in Fig. 2. The modulation depth and

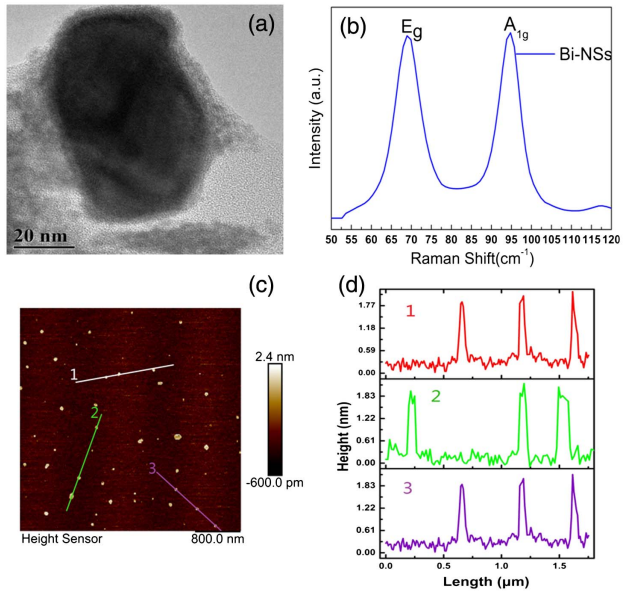

Fig. 1. (a) HRTEM image, (b) Raman spectrum, (c) AFM image of the bismuth nanosheets, and (d) typical height profiles.

saturation fluence are found to be 1.82% and 3.59 kW/cm^2, respectively. Considering the Fresnel reflection loss of the JGS3 substrate, the nonsaturable loss of the Bi-NSs SA was calculated to be about 3.7%.

A schematic of the experimental device is shown in Fig. 3. The pump source was a commercial 972 nm fiber-coupled LD with a core diameter of about 50 μm and a numerical aperture (NA) of 0.15. The pump light was transmitted through the fiber and expanded into the gain medium by a coupling system of 1:2. The 3 at. % Er^{3+}:SrF_2 crystal was grown by the traditional Bridgman method, which is described in detail in Ref. [42]. The uncoated Er^{3+}:SrF_2 crystal was mounted on a copper block stabilized at 12°C by cycling cooling water. The laser resonator consists of a concave mirror (IM) and a plane output coupler (OC), with a physical length of about 48 mm. The IM with a 100 mm radius of curvature was antireflection coated for 974 nm and high-reflection coated for 2.7–2.95 μm. For the OC, we used different coated plane mirrors with transmissions of 1%, 3%, and 5% for 2.7–2.95 μm.

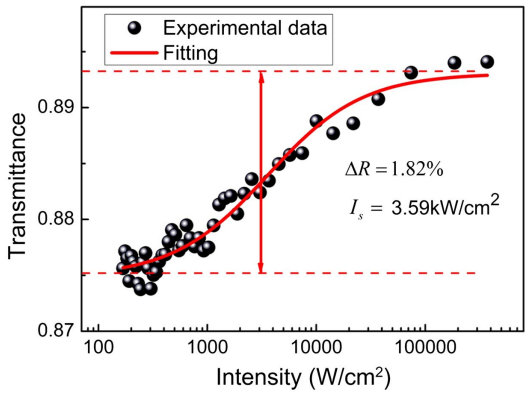

Fig. 2. Nonlinear transmission of Bi-NSs SA.

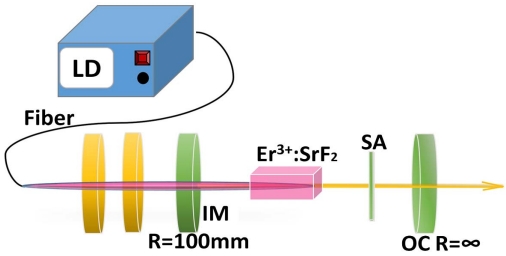

Fig. 3. Schematic of the passively Q-switched Er^{3+}:SrF_2 laser with a Bi-NSs SA.

3. RESULTS AND DISCUSSION

Continuous-wave (CW) laser operation was first carried out with different OC transmissions, and the average output powers are shown in Fig. 4. With an OC transmission of 3% at an absorbed pump power of 1.97 W, a maximum output power of 393 mW and corresponding slope efficiency of 21.3% were obtained. The Bi-NSs were used as the SA and inserted into the resonator to operate the laser in the passively Q-switched regime. By carefully adjusting the position and angle of the Bi-NSs SA, the output laser displayed stable pulse repetition rates and uniform pulse trains when the absorbed pump power reached about 1 W. Under the same incident pump power and OC transmission, the maximum average output power was 226 mW, with a slope efficiency of 13.6%. Figure 5 shows the Q-switched output power as a function of the absorbed pump power with different OC transmissions. The inset (a) shows the fluctuation of the maximum output power was about 8.4% for 70 min detection. Figures 6(a) and 6(b) display the laser beam profile and light intensity distribution, respectively, which were recorded by a detector (NS2-Pyro/9/5-PRO, Photon). The results indicate that the generated beam has an excellent TEM_{00} transversal profile.

The pulse repetition rate, pulse duration, single-pulse energy, and peak power as functions of the absorbed pump power for different OC transmissions are shown in Figs. 7(a)–7(d). With increasing absorbed pump power, the repetition rate and peak power increased and the pulse duration gradually decreased. The maximum output power, pulse repetition rate, pulse duration, single-pulse energy, peak power, and wavelength under different OC mirrors were recorded at the absorbed power of 1.97 W and are detailed in Table 1. According to these results, the best OC transmission is around

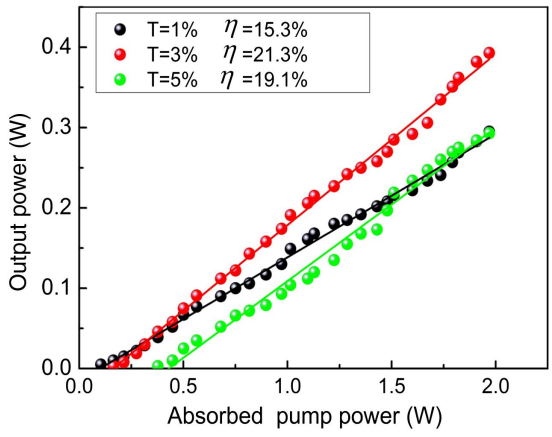

Fig. 4. CW output power versus the absorbed pump power for different OC transmissions.

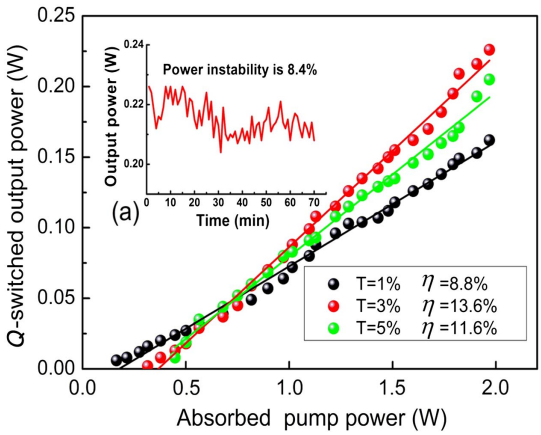

Fig. 5. Q-switched output power versus the absorbed pump power for different OC transmissions. Inset (a) shows the maximum output power versus time.

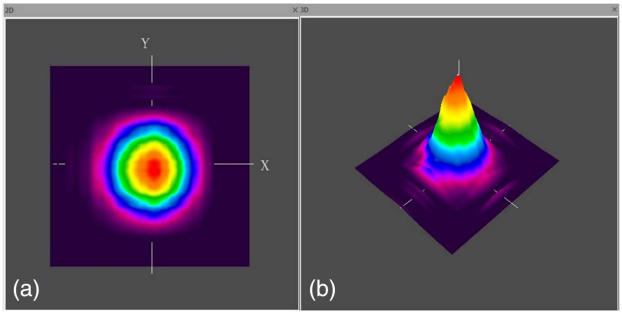

Fig. 6. (a) Laser beam profile and (b) 3D light intensity distribution recorded at the maximum output power for the Q-switched laser.

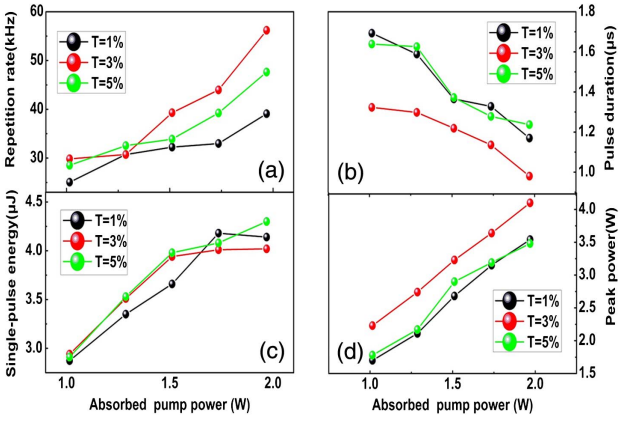

Fig. 7. (a) Pulse repetition rate, (b) pulse duration, (c) single-pulse energy, and (d) peak power versus the absorbed pump power for different OC transmissions.

Table 1. Experimental Results Achieved under Different OC Mirrors

OC Transmission	Max. Output Power (mW)	Repetition Rate (kHz)	Pulse Width (ns)	Single-Pulse Energy (μJ)	Peak Power (W)	Wavelength (nm)
1%	162	39.1	1170	4.14	3.54	2799.1
3%	226	56.2	980	4.02	4.10	2730.5 + 2752.2
5%	205	47.6	1237	4.30	3.48	2732.6 + 2737.0

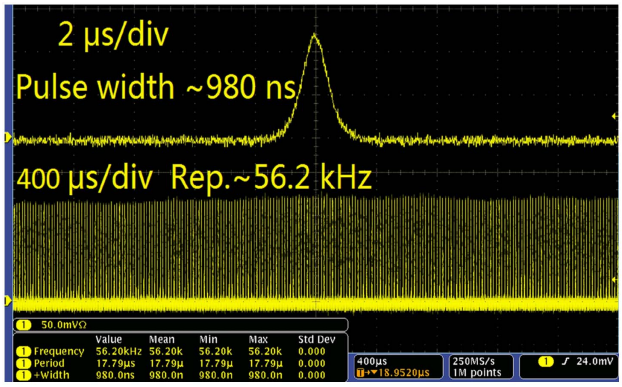

Fig. 8. *Q*-switched pulse trains recorded at 2 and 400 μs/div, under an absorbed pump power of 1.97 W for the OC transmission of 3%.

3% under the same conditions. Figure 8 shows the typical pulse trains recorded at different time scales by a digital oscilloscope (Tektronix DPO4104, 1 GHz bandwidth). At the maximum absorbed pump power, the repetition rate recorded at 400 μs/div was 56.2 kHz and the single-pulse duration recorded at 2 μs/div was 980 ns.

Figure 9 shows the reliability of the laser emission spectra recorded under the OC transmission of 3% by an optical spectrum analyzer (MS3504i). The central wavelengths are 2729.5 and 2751.7 nm for the CW laser, and the full width at half-maximum (FWHM) are 0.70 and 1.0 nm following a Gaussian fit. The laser emission spectrum is consistent with the emission spectrum of the Er^{3+}:SrF_2 crystal reported in Ref. [42], which exhibits two emission peaks around 2727 and 2745 nm. The simultaneous dual-wavelength laser can

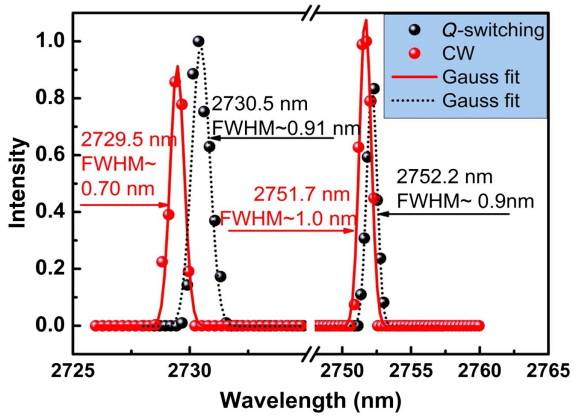

Fig. 9. Optical spectra recorded in the CW regime and *Q*-switched regime for OC transmission of 3%.

be used as a light source for the generation of terahertz emission [43]. For the *Q*-switched laser operation, the central wavelengths are 2730.5 and 2752.2 nm and the corresponding FWHM are 0.91 and 0.9 nm, respectively. A redshift in the lasing wavelength was observed. Reference [44] describes the cause of the phenomenon in detail. The short wavelengths located near the emission peaks are more likely to oscillate for the CW laser. When inserting Bi-NSs into the cavity, the insertion loss of the fused quartz substrate was high and the gain at different wavelengths was discrepant, so the wavelength shifted toward either longer or shorter wavelengths [45]. As the intracavity loss changed, the Stark energy levels of Er^{3+} split and the laser energy level (Er^{3+}:$^4I_{11/2}$) were lowered. The residual population did not decrease efficiently in the lower laser energy level (Er^{3+}:$^4I_{13/2}$) as the level has a longer lifetime. Therefore, the laser would oscillate at longer wavelengths.

4. CONCLUSION

In conclusion, we successfully demonstrated the first, to the best of our knowledge, dual-wavelength passively *Q*-switched Er^{3+}:SrF_2 laser at 2730.5 and 2752.2 nm, with Bi-NSs as the SA. For an absorbed pump power of 1.97 W, a maximum average output power of 226 mW was achieved. The shortest pulse duration of 980 ns was obtained with a repetition rate of 56.2 kHz, corresponding to a single-pulse energy of 4.02 μJ and a peak power of 4.1 W. The results indicate that Bi-NSs, which are affordable and can be easily prepared, exhibit reliable and excellent features as a promising SA for pulse lasers in the mid-infrared region.

Funding. National Natural Science Foundation of China (NSFC) (61475089, 61435010, 61635012); Development Projects of Shandong Province Science and Technology (2017GGX30102); National Key Research and Development Program of China (2016YFB0701002); Science and Technology Planning Project of Guangdong Province (2016B050501005); Science and Technology Innovation Commission of Shenzhen (KQTD2015032416270385).

REFERENCES

1. Y. P. Peng, B. X. Jiang, J. T. Fan, X. Q. Yuan, and L. Zhang, "Review of in mid-infrared laser materials directly pumped by laser-diode," Laser Optoelectron. Prog. **52**, 020001 (2015).
2. A. Godard, "Infrared (2–12 μm) solid-state laser sources: a review," C. R. Physique **8**, 1100–1128 (2007).
3. J. Liu, Y. G. Wang, Z. S. Qu, and X. W. Fan, "2 μm passive *Q*-switched mode-locked Tm^{3+}:YAP laser with single-walled carbon nanotube absorber," Opt. Laser Technol. **44**, 960–962 (2012).
4. K. Scholle, E. Heumann, and G. Huber, "Single mode Tm and Tm, Ho:LuAG lasers for LIDAR applications," Laser Phys. Lett. **1**, 285–290 (2004).

5. W. W. Ma, L. B. Su, X. D. Xu, J. Y. Wang, D. P. Jiang, L. H. Zheng, X. W. Fan, C. Li, J. Liu, and J. Xu, "Effect of erbium concentration on spectroscopic properties and 2.79 μm laser performance of Er:CaF_2 crystals," Opt. Mater. Express **6**, 409–415 (2016).
6. Z. Y. Yan, G. Q. Li, T. Li, S. Z. Zhao, K. J. Yang, S. Y. Zhang, M. Q. Fan, L. Guo, and B. T. Zhang, "Passively *Q*-switched Ho, Pr:$LiLuF_4$ laser at 2.95 μm using $MoSe_2$," IEEE Photon. J. **9**, 1506207 (2017).
7. H. K. Nie, P. X. Zhang, B. T. Zhang, K. J. Yang, L. H. Zhang, T. Li, S. Y. Zhang, J. Q. Xu, Y. Hang, and J. L. He, "Diode-end-pumped Ho, Pr:$LiLuF_4$ bulk laser at 2.95 μm," Opt. Lett. **42**, 699–702 (2017).
8. S. Tokita, M. Murakami, S. Shimizu, M. Hashida, and S. Sakabe, "Liquid-cooled 24 W mid-infrared Er:ZBLAN fiber laser," Opt. Lett. **34**, 3062–3064 (2009).
9. J. J. Liu, X. W. Fan, J. Liu, W. W. Ma, J. Y. Wang, and L. Su, "Mid-infrared self-*Q*-switched Er, Pr:CaF_2 diode-pumped laser," Opt. Lett. **41**, 4660–4663 (2016).
10. Y. Y. Guo, Y. Tian, L. Y. Zhang, L. L. Hu, N. K. Chen, and J. J. Zhang, "Pr^{3+}-sensitized Er^{3+}-doped bismuthate glass for generating high inversion rates at 2.7 μm wavelength," Opt. Lett. **37**, 3387–3389 (2012).
11. H. Lin, D. Q. Chen, Y. L. Yu, A. P. Yang, and Y. S. Wang, "Enhanced mid-infrared emissions of Er^{3+} at 2.7 μm via Nd^{3+} sensitization in chalcohalide glass," Opt. Lett. **36**, 1815–1817 (2011).
12. W. W. Ma, X. B. Qian, J. Y. Wang, J. J. Liu, X. W. Fan, J. Liu, L. B. Su, and J. Xu, "Highly efficient dual-wavelength mid-infrared CW laser in diode end-pumped Er:SrF_2 single crystals," Sci. Rep. **6**, 36635 (2016).
13. J. J. Liu, J. Liu, J. M. Yang, W. W. Ma, Q. H. Wu, and L. B. Su, "Efficient mid-infrared laser under different excitation pump wavelengths," Opt. Lett. **42**, 3908–3911 (2017).
14. H. T. Zhu, L. N. Zhao, J. Liu, S. C. Xu, W. Cai, S. Z. Jiang, L. H. Zheng, L. B. Su, and J. Xu, "Monolayer graphene saturable absorber with sandwich structure for ultrafast solid-state laser," Opt. Eng. **55**, 081304 (2016).
15. M. Q. Fan, T. Li, G. Q. Li, S. Z. Zhao, K. J. Yang, S. Y. Zhang, B. T. Zhang, J. Q. Xu, and C. Krankel, "Passively *Q*-switched Ho, Pr:$LiLuF_4$ laser with graphitic carbon nitride nanosheet film," Opt. Express **25**, 12796–12803 (2017).
16. H. T. Zhu, W. Cai, J. F. Wei, J. Liu, L. H. Zheng, L. B. Su, J. Xu, and Y. G. Wang, "763 fs passively mode-locked Yb:Y_2SiO_5 laser with a graphene oxide absorber mirror," Opt. Laser Technol. **68**, 120–123 (2015).
17. Q. Bao, H. Zhang, Y. Wang, Z. Ni, Y. Yan, Z. Shen, K. Loh, and D. Tang, "Atomic-layer graphene as a saturable absorber for ultrafast pulsed lasers," Adv. Funct. Mater. **19**, 3077–3083 (2009).
18. X. F. Guan, L. J. Zhan, Z. W. Zhu, B. Xu, H. Y. Xu, Z. P. Cai, W. W. Cai, X. D. Xu, J. Zhang, and J. Xu, "Continuous-wave and CVD-graphene-based passively *Q*-switched Er:Y_2O_3 ceramic lasers at 2.7 μm," Appl. Opt. **57**, 371–376 (2018).
19. C. Zhang, J. Liu, X. W. Fan, Q. Q. Peng, X. S. Guo, D. P. Jiang, X. B. Qian, and L. B. Su, "Compact passive *Q*-switching of a diode-pumped Tm, Y:CaF_2 laser near 2 μm," Opt. Laser Technol. **103**, 89–92 (2018).
20. L. Guo, T. Li, S. Y. Zhang, M. J. Wang, S. Z. Zhao, K. J. Yang, D. C. Li, and Z. Y. Yan, "Passively *Q*-switched Ho, Pr:$LiLuF_4$ bulk laser at 2.95 μm using WS_2 saturable absorbers," Opt. Mater. Express **7**, 2090–2095 (2017).
21. S. Y. Zhang, X. X. Liu, L. Guo, M. Q. Fan, F. Lou, P. Gao, G. H. Guo, J. L. Yang, J. J. Liu, T. Li, K. J. Yang, S. Z. Zhao, J. Liu, J. Q. Xu, and Y. Hang, "Passively *Q*-switched Ho, Pr:LLF bulk slab laser at 2.95 μm based on MoS_2 saturable absorber," IEEE Photon. Tech. Lett. **29**, 2258–2261 (2017).
22. P. G. Ge, J. Liu, S. Z. Jiang, Y. Y. Xu, and B. Y. Man, "Compact *Q*-switched 2 μm Tm:$GdVO_4$ laser with MoS_2 absorber," Photon. Res. **3**, 256–259 (2015).
23. X. C. Su, B. T. Zhang, Y. R. Wang, G. B. He, G. R. Li, N. Lin, K. J. Yang, J. L. He, and S. D. Liu, "Broadband rhenium disulfide optical modulator for solid-state lasers," Photon. Res. **6**, 498–505 (2018).
24. C. J. Zhao, Y. H. Zou, Y. Chen, Z. T. Wang, S. B. Lu, H. Zhang, S. C. Wen, and D. Y. Tang, "Wavelength-tunable picosecond soliton fiber laser with topological insulator: Bi_2Se_3 as a mode locker," Opt. Express **20**, 27888–27895 (2012).
25. J. P. Qiao, S. Z. Zhao, K. J. Yang, W. H. Song, W. C. Qiao, C. L. Wu, J. Zhao, G. Q. Li, D. C. Li, T. Li, H. Liu, and C. K. Lee, "High-quality 2-μm *Q*-switched pulsed solid-state lasers using spin-coating-coreduction approach synthesized Bi_2Te_3 topological insulators," Photon. Res. **6**, 314–320 (2018).
26. H. Yu, H. Zhang, Y. Wang, C. Zhao, B. Wang, S. Wen, H. Zhang, and J. Wang, "Topological insulator as an optical modulator for pulsed solid-state lasers," Laser Photon. Rev. **7**, L77–L83 (2013).
27. X. Liu, K. Yang, S. Zhao, T. Li, W. Qiao, H. Zhang, B. Zhang, J. He, J. Bian, L. Zheng, L. Su, and J. Xu, "High-power passively *Q*-switched 2 μm all-solid-state laser based on a Bi_2Te_3 saturable absorber," Photon. Res. **5**, 461–466 (2017).
28. Z. Luo, Y. Huang, J. Weng, H. Cheng, Z. Lin, B. Xu, Z. Cai, and H. Xu, "1.06 μm *Q*-switched ytterbium-dope fiber laser using few-layer topological insulator Bi_2Se_3 as a saturable absorber," Opt. Express **21**, 29516–29522 (2013).
29. J. J. Liu, J. Liu, Z. N. Guo, H. Zhang, W. W. Ma, J. Y. Wang, and L. B. Su, "Dual-wavelength *Q*-switched Er:SrF_2 laser with a black phosphorus absorber in the mid-infrared region," Opt. Express **24**, 30289–30295 (2016).
30. Z. N. Guo, H. Zhang, S. B. Lu, Z. T. Wang, S. Y. Tang, J. D. Shao, Z. B. Sun, H. H. Xie, H. Y. Wang, X. F. Yu, and P. K. Chu, "From black phosphorus to phosphorene: basic solvent exfoliation, evolution of Raman scattering, and applications to ultrafast photonics," Adv. Funct. Mater. **25**, 6996–7002 (2015).
31. B. T. Zhang, F. Lou, R. W. Zhao, J. L. He, J. Li, X. C. Su, J. Ning, and K. J. Yang, "Exfoliated layers of black phosphorus as saturable absorber for ultrafast solid-state laser," Opt. Lett. **40**, 3691–3694 (2015).
32. X. Su, Y. Wang, B. Zhang, R. Zhao, K. Yang, J. He, Q. Hu, Z. Jia, and X. Tao, "Femtosecond solid-state laser based on a few-layered black phosphorus saturable absorber," Opt. Lett. **41**, 1945–1948 (2016).
33. Y. Xu, Z. Wang, Z. Guo, H. Huang, Q. Xiao, H. Zhang, and X. F. Yu, "Solvothermal synthesis and ultrafast photonics of black phosphorus quantum dots," Adv. Opt. Mater. **4**, 1223–1229 (2016).
34. Y. Song, S. Chen, Q. Zhang, L. Li, L. Zhao, H. Zhang, and D. Tang, "Vector soliton fiber laser passively mode locked by few layer black phosphorus-based optical saturable absorber," Opt. Express **24**, 25933–25942 (2016).
35. X. T. Jiang, S. X. Liu, W. Y. Liang, S. J. Luo, Z. L. He, Y. Q. Ge, H. D. Wang, R. Cao, F. Zhang, Q. Wen, J. Q. Li, Q. L. Bao, D. Y. Fan, and H. Zhang, "Broadband nonlinear photonics in few-layer MXene $Ti_3C_2T_x$ (T = F, O, or OH)," Laser Photon. Rev. **12**, 1700229 (2018).
36. L. Lu, X. Tang, R. Cao, L. Wu, Z. Li, G. Jing, B. Dong, S. Lu, Y. Li, Y. Xiang, J. Li, D. Fan, and H. Zhang, "Broadband nonlinear optical response in few-layer antimonene and antimonene quantum dots: a promising optical Kerr media with enhanced stability," Adv. Opt. Mater. **5**, 1700301 (2017).
37. Y. Song, Z. Liang, X. Jiang, Y. Chen, Z. Li, L. Lu, Y. Ge, K. Wang, J. Zheng, S. Lu, J. Ji, and H. Zhang, "Few-layer antimonene decorated microfiber: ultra-short pulse generation and all-optical thresholding with enhanced long term stability," 2D Mater. **4**, 045010 (2017).
38. Y. Guo, F. Pan, M. Ye, X. T. Sun, Y. Y. Wang, J. Z. Li, X. Y. Zhang, H. Zhang, Y. Y. Pan, Z. G. Song, J. B. Yang, and J. Lu, "Monolayer bismuthene-metal contacts: a theoretical study," ACS Appl. Mater. Inter. **9**, 23128–23140 (2017).
39. L. Lu, Z. M. Liang, L. M. Wu, Y. X. Chen, Y. F. Song, S. C. Dhanabalan, J. S. Ponraj, B. Q. Dong, Y. J. Xiang, F. Xing, D. Y. Fan, and H. Zhang, "Few-layer bismuthene: sonochemical exfoliation, nonlinear optics and applications for ultrafast photonics with enhanced stability," Laser Photon. Rev. **12**, 1700221 (2017).
40. P. Kumar, J. Singh, and A. C. Pandey, "Rational low temperature synthesis and structural investigations of ultrathin bismuth nanosheets," RSC Adv. **3**, 2313–2317 (2013).

41. S. B. Lu, L. L. Miao, Z. N. Guo, X. Qi, C. J. Zhao, H. Zhang, S. C. Wen, D. Y. Tang, and D. Y. Fan, "Broadband nonlinear optical response in multilayer black phosphorus: an emerging infrared and mid-infrared optical material," Opt. Express **23**, 11183–11194 (2015).
42. L. B. Su, X. S. Guo, D. P. Jiang, Q. H. Wu, Z. P. Qin, and G. Q. Xie, "Highly-efficient mid-infrared CW laser operation in a lightly-doped 3 at.% Er:SrF_2 single crystal," Opt. Express **26**, 5558–5563 (2018).
43. W. L. Gao, J. Ma, G. Q. Xie, J. Zhang, D. W. Luo, H. Yang, D. Y. Tang, J. Ma, P. Yuan, and L. J. Qian, "Highly efficient 2 μm Tm:YAG ceramic laser," Opt. Lett. **37**, 1076–1078 (2012).
44. L. Wang, H. T. Huang, D. Y. Shen, J. Zhang, H. Chen, Y. Wang, X. Liu, and D. Y. Tang, "Room temperature continuous-wave laser performance of LD pumped Er:Lu_2O_3 and Er:Y_2O_3 ceramic at 2.7 μm," Opt. Express **22**, 19495–19503 (2014).
45. Y. Chen, C. J. Zhao, S. Q. Chen, J. Du, P. H. Tang, G. B. Jiang, H. Zhang, S. C. Wen, and D. Y. Tang, "Large energy, wavelength widely tunable, topological insulator *Q*-switched erbium-doped fiber laser," IEEE J. Sel. Top. Quantum **20**, 0900508 (2014).